

Title: Decoding Heterogenous Single-cell Perturbation Responses

Bicna Song^{1,2}, Dingyu Liu^{3,4}, Weiwei Dai^{5,6}, Natalie McMyn⁵, Qingyang Wang⁷, Dapeng Yang³, Adam Krejci⁸, Anatoly Vasilyev⁸, Nicole Untermoser⁸, Anke Loregger⁸, Dongyuan Song⁹, Breanna Williams³, Bess Rosen^{3,10}, Xiaolong Cheng^{1,2}, Lumen Chao^{1,2}, Hanuman Kale³, Hao Zhang⁵, Yarui Diao¹¹, Tilmann Bürckstümmer⁸, Jenet M. Siliciano⁵, Jingyi Jessica Li^{7,9,12-14}, Robert Siliciano^{5,6}, Danwei Huangfu³, Wei Li^{1,2,#}

1 Center for Genetic Medicine Research, Children's National Hospital, Washington DC, USA

2 Department of Genomics and Precision Medicine, George Washington University, Washington DC, USA

3 Developmental Biology Program, Sloan Kettering Institute, New York City, NY, USA

4 Louis V. Gerstner Jr. Graduate School of Biomedical Sciences, Memorial Sloan Kettering Cancer Center, New York City, NY, USA.

5 Department of Medicine, Johns Hopkins University School of Medicine, Baltimore, MD, USA

6 Howard Hughes Medical Institute, Johns Hopkins University School of Medicine, Baltimore, MD, USA.

7 Department of Statistics and Data Science, University of California, Los Angeles, CA, USA

8 Myllia Biotechnology GmbH. Am Kanal 27, 1110 Vienna Austria.

9 Bioinformatics Interdepartmental Ph.D. Program, University of California, Los Angeles, CA, USA

10 Weill Cornell Graduate School of Medical Sciences, Weill Cornell Medicine, New York, NY, USA.

11 Department of Cell Biology, Duke University Medical Center, Durham, NC, USA

12 Department of Human Genetics, University of California, Los Angeles, CA, USA

13 Department of Biostatistics, University of California, Los Angeles, CA, USA

14 Department of Computational Medicine, University of California, Los Angeles, CA, USA

Correspondences should be addressed. wli2@childrensnational.org;

One sentence summary: We present a method to quantify diverse perturbation responses and discover novel biological insights in single-cell perturbation datasets.

Keywords: Perturb-seq, CRISPR-based genetic perturbations, single-cell RNA-seq, computational model

Abstract

Understanding the diverse responses of individual cells to the same perturbation is central to many biological and biomedical problems. Current methods, however, fall short in precisely quantifying the heterogenous perturbation responses and, more importantly, unveiling new biological insights from such heterogeneity. Here we introduce the “Perturbation Score” (PS) method, based on constrained quadratic optimization, to quantify diverse perturbation responses at a single-cell level. Applied to single-cell transcriptomes of large-scale genetic perturbation datasets (e.g., Perturb-seq), PS outperforms existing methods in quantifying partial gene perturbation responses. In addition, PS presents two major advances over existing methods. First, PS enables large-scale, single-cell resolution dosage analysis of perturbation, without the need to titrate perturbation strength. By analyzing the dosage-response patterns of over 2,000 essential genes in Perturb-seq, we identify two distinct patterns, depending on whether a moderate reduction in their expression induces strong downstream expression alterations. Second, PS

identifies intrinsic and extrinsic biological determinants for perturbation responses. We demonstrate the application of PS in various contexts like T cell stimulation, latent HIV-1 expression, and pancreatic cell differentiation. Notably, PS unveiled a previously unrecognized, cell-type specific role of CCDC6 (coiled-coil domain containing 6) in guiding liver and pancreatic lineage decisions, where CCDC6 knockouts drives the endoderm cell differentiation towards liver lineage, rather than pancreatic lineage. Collectively, our PS approach provides an innovative methodology to perform dosage-to-function analysis and foster new biological discoveries from single-cell perturbation datasets.

Introduction

Perturbation is essential for understanding the functions of mammalian genome that encodes protein-coding genes and non-coding elements (e.g., enhancers). Single-cell profiling of cells undergoing genetic, chemical, environmental or mechanical perturbations is commonly used to profile perturbation responses at a single-cell level. Recently, high-throughput approaches using single-cell RNA-seq (scRNA-seq) as the readout of perturbation have been developed, including multiplexing of perturbations and single-cell CRISPR screen¹⁻⁷. Furthermore, this concept has been extended to study changes in single-cell chromatin accessibility^{8,9}, spatial transcriptomics¹⁰ upon perturbations or perturbation combinations¹¹⁻¹³, etc.

Understanding how perturbations lead to diverse responses within cells is critical to understanding the fundamental biology behind perturbation. The heterogeneity of perturbation response is driven by technical and (perhaps more interestingly) biological factors (**Fig. 1a**). Technical factors, including single-cell assays used to profile the response and the on-target/off-target effects of perturbations, are known drivers that lead to differences of single-cell profiles in the data¹⁴⁻¹⁶. In contrast, multiple biological factors also control the responses of perturbations. These factors may be either intrinsic (e.g., the activities of other coding-and non-coding genomic elements) or extrinsic (e.g., cell states or types, environment factors), all of which define the context of perturbation response. For example, combined expressions of transcription factors (TFs) are critical for many cellular state conversions. Therefore, to properly decode the functions of these TFs via perturbation, one must consider the effect of cell state and the activities of other companion TFs. For this reason, defining the heterogeneity of perturbation outcomes, and identifying factors that contribute to these outcomes, will be important to understand how cells respond to perturbation.

Unfortunately, computational frameworks are currently lacking to decode the diverse outcomes of perturbations. For technical factors, mixscape is the only method that detect and mitigate confounding variations (e.g., incomplete knockouts from CRISPR/Cas9)¹⁶. However, its performance has not been rigorously benchmarked, especially when partial gene functions are perturbed using techniques like CRISPR interference (CRISPRi). More importantly, no methods have been developed to unveil new biological insights from the heterogenous perturbation outcomes, including discovering biological determinants that govern differential perturbation responses.

Here we present a computational framework, named Perturbation Score (PS), to detect heterogenous perturbation outcomes in single-cell transcriptomics datasets. The PS score, estimated from constrained quadratic optimization, quantitatively measures the strength of perturbation outcome at a single cell level. We performed comprehensive benchmark studies that demonstrated the outstanding performance of PS over existing methods, including simulated datasets, genome-scale Perturb-seq, and published

Perturb-seq datasets that cover various CRISPR-based technologies. More importantly, PS presents two major conceptual advances in analyzing single-cell perturbation data: the dosage analysis of perturbation, and the identification of novel biological determinants that govern the heterogeneity of perturbation responses. First, we performed dosage-dependent analysis of perturbing essential genes, and reveals two different patterns of dosage-response, depending on whether moderate perturbation leads to strong expression changes of downstream genes. Second, we identified intrinsic and extrinsic biological factors governing critical gene functions in latent HIV-1 expression and pancreatic/liver development. In particular, we identified and confirmed a novel function of CCDC6 whose perturbation drives duodenum cell differentiation towards liver commitment, based on the findings enabled by the PS score of CCDC6. Collectively, our PS framework provides a powerful model to decode heterogenous perturbation outcomes from single-cell assays.

Results

A Perturbation Score (PS) to detect heterogenous perturbation outcomes within and across datasets.

Perturbing the same gene (or non-coding elements) may result in different phenotypic changes or transcriptional outcomes (**Fig. 1a**), depending on different factors including technical (e.g., perturbation efficiency) and biological (e.g., cell type, cell state, activities of cofactors). Unfortunately, existing methods are limited to detecting only technical factors¹⁶, while biological factors remain unexplored. To bridge this gap, we built a computational framework to describe the continuum of perturbation outcomes in single-cell datasets using scRNA-seq as readout. Corresponding assays include single-cell CRISPR screens (e.g., Perturb-seq), or simply multiplex scRNA-seq profiling of various perturbations (e.g., sci-Plex; **Fig. 1b, c**). We define a score, named Perturbation Score (or PS), to quantitatively measure the strength of perturbation, where PS=0 score indicates no perturbation effect (e.g., effects corresponding to unperturbed, wild-type gene functions). In contrast, PS=1 indicates the maximum perturbation effect observed within a dataset; for example, effects that correspond to homozygous knockouts on both alleles of a gene. We utilize the expressions of multiple downstream targets of a perturbed gene to infer the (unknown) values of PS score (**Fig. 1b**). For example, if one cell has dramatic expression changes on the known downstream target genes, then the value of PS should be close to 1. Otherwise, PS should be close to 0.

We built a computational model, based on a constrained quadratic optimization, to automatically identify the downstream targets of perturbed genes and calculate PS scores (**Fig. 1c**). This PS framework, named “scMAGECK-PS”, is based on our previously published scMAGECK algorithm¹⁵ and consists of three steps. First, scMAGECK-PS identifies differentially expressed genes (DEGs) upon perturbation (e.g., perturbing the function of gene X), by comparing the transcriptome profiles between perturbed cells and unperturbed cells. These DEGs are served as “signature” target genes of X. Second, scMAGECK-PS used a previously developed scMAGECK model to estimate the average effect of perturbation on these target genes, which can be estimated from the first step. Third, scMAGECK-PS uses a constraint optimization procedure to find the value of PS that minimizes the sum of mean squared errors between predicted and measured expression changes of all downstream targets (see Methods). The constraints are established such that any PS score is non-negative for cells with X perturbed, and is exactly zero in cells without perturbation. Such constraints can be established based on the prior information of perturbations; for example, the expression matrix of single-guide RNAs (sgRNAs).

PS outperforms mixscape in quantifying partial perturbations.

mixscape¹⁶ is currently the only method to detect and remove technical factors that affect perturbation outcome, especially incomplete gene knockouts that are generated from CRISPR/Cas9. However, the performance of mixscape on partial gene perturbations have not been fully evaluated. Here we compared PS with mixscape using multiple benchmark datasets. We first used synthetic datasets to evaluate the performances of different methods, because finding a real scRNA-seq dataset that contains ground truth (*i.e.*, accurate measurements of loss-of-function upon perturbation) is challenging. For synthetic data generation, we used scDesign3¹⁷ to simulate the single-cell transcriptomic responses upon perturbing the 50% and 100% functions of Nelfb, based on a real scRNA-seq dataset that deletes Nelfb in mouse T cells¹⁸ (**Supplementary Fig. S1a**; see Methods). We specified different numbers of DEG genes (from 10 to 500), and simulated their expression changes upon 50% or 100% perturbations of Nelfb functions. In all the cases, PS correctly estimated partial perturbation, where the median PS scores range from 0.32-0.34 for 50% perturbation, and greater than 0.8 for 100% perturbation, respectively (**Fig. 1d-e**; **Supplementary Fig. S1b-e**). In contrast, mixscape uniformly assigned the posterior probability of perturbation to 1 in all the cases, an indication that mixscape is not suited to analyze the outcome of partial gene perturbations (**Fig. 1d-e**; **Supplementary Fig. S1b-e**), possibly due to the bimodal statistic model it used that only considers 100% knockout effects¹⁶.

We next evaluate different methods using real single-cell perturbation datasets. We chose CRISPR interference (CRISPRi)-based Perturb-seq datasets (**Fig. 1f-i**), because the CRISPRi system directly modulates the expression levels of perturbed genes, and the perturbation efficiency can be accessed using single-cell transcriptomic data. Two published K562 CROP-seq datasets are used¹⁹, where only 1 gRNA is expressed within each cell (*i.e.*, low Multiplicity of Infection or MOI) in one dataset, and multiple gRNAs are expressed (*i.e.*, high MOI) in another dataset. We examine cells where the transcription starting sites (TSS) of highly expressed protein-coding genes are targeted (23 and 342 genes, respectively; **Fig. 1g-i**, **Supplementary Fig. S1f-g**). If the TSS of gene *X* is perturbed, we first remove the expression of *X* from expression matrix, and use the rest of gene expressions to measure the perturbation efficiency of *X*. The scores of different methods are then compared with the expression of *X*, which is a direct measurement of perturbation efficiency (**Fig. 1f**). In over 40% of these genes (10 out of 23 for low MOI, 139 out of 342 for high MOI), PS score has a strong negative correlation with the expression of *X* (**Fig. 1g**), defined as Pearson correlation coefficient < -0.1 and *p* value < 0.01 . In contrast, mixscape scores correlate with *X* expression in none of the genes (for low MOI dataset; **Fig. 1g**), or in less than 5% of all the genes (for high MOI dataset; **Supplementary Fig. S1f-g**). PS detects a much greater number of cells that have a strong perturbation effect (PS or mixscape score > 0.5 ; **Fig. 1h**), whose scores are strongly negatively correlated with gene expression (**Fig. 1i**). We also tested both methods in another CRISPRi-based Perturb-seq dataset, where sgRNAs with mismatches reduce their efficiencies, leading to partial perturbation effects²⁰ (**Supplementary Fig. S1h-i**). PS has a high sensitivity and a good balance between sensitivity and specificity, evidenced by the higher values of Pearson correlation coefficient (**Supplementary Fig. S1h**) and Areas Under the ROC Curve (AUC) values (**Supplementary Fig. S1i**).

To further benchmark different methods in terms of a phenotype of interest, we designed and performed a genome-scale CRISPRi Perturb-seq on both unstimulated and stimulated Jurkat, a T lymphocyte cell model (**Fig. 2a**), and evaluated the performances of different methods in identifying known regulators of T cell activation. We designed Perturb-seq library that contains sgRNAs targeting the TSS of 18,595 genes (4-6 guides per gene), and used a TAP-seq-based²¹, multiplex primer panel to detect the expressions of 374 genes with high sensitivity (see **Supplementary Table S1** and Methods). We

obtained high-quality scRNA-seq data of over 586,000 single cells after quality control, and the UMAP clustering of Perturb-seq datasets clearly demonstrated the differences between stimulated and non-stimulated cells (**Fig. 2b**). Next, we ran PS or mixscape to calculate the scores of all perturbations at a single-cell level; and for each perturbed gene, we calculated its overall perturbation score, by adding the scores of all cells that express a corresponding sgRNA targeting that gene. Because our system focuses on T cell stimulation, perturbing a gene that reaches a highest (and lowest) cumulative score should have the strongest (and no) effect on T cell stimulation, respectively. For an independent evaluation, we extracted 385 (and 1297) positive (and negative) hits whose perturbation impairs (or does not impair) the stimulation of T cells from a published genome-scale CRISPR screen²², respectively. Both Perturb-seq and pooled CRISPR screen identified many known positive regulators of T cell activation, such as components of the T cell receptor complex (e.g., CD3D) and proximal signaling components (e.g., LCK; **Fig. 2c**). The distribution of the perturbation scores estimated by PS or mixscape is skewed towards cells corresponding to non-stimulating state, in concordance with their negative selections in pooled CRISPR screens using T cell stimulation as readout (**Fig. 2c; Supplementary Fig. S2**). However, when comparing the receiver-operating characteristic (ROC) score, PS reaches a higher Area Under the ROC (AUC) score than mixscape (**Fig. 2d**), indicating its better performance in accurately separating positive from negative hits.

Finally, we tested different methods on a published ECCITE-seq, which simultaneously measures single-cell transcriptomes, surface proteins, and perturbations¹⁶. PDL1 protein expression was used as an independent metric of evaluation (**Fig. 2e**), because PDL1 is a well-studied gene whose protein expression is well understood. Among 25 perturbed genes in ECCITE-seq perturbation library, 17 of those are known factors to regulate PDL1 expression (**Fig. 2f**). We compared PS with mixscape in terms of predicting changes in PDL1 expression (**Fig. 2f; Supplementary Fig. S3**). In addition, the expression of the perturbed gene is also included in the comparison as a naïve method. In 19 out of 25 genes (76%), PS outperformed mixscape and perturbed gene expression in predicting PDL1 expression (**Fig. 2e**), including 12 out of 17 (71%) known PDL1 regulators. Notably, for genes whose perturbations led to strong transcriptomic changes (e.g., IFNGR1, IFNGR2, JAK2, STAT1), both PS and mixscape work well, reaching over 0.8 AUC value (**Fig. 2f**). For other genes whose perturbation only leads to moderate or weak expression changes, as is revealed from the original study¹⁶, PS outperforms mixscape, including those that are confirmed to be PDL1 regulators (*i.e.*, genes marked in red in **Fig. 2f**).

Analyzing dosage-dependent effects of perturbation.

Traditionally, dosage analysis requires a careful, time-consuming adjustment of perturbation strength, including changing drug concentrations or designing sgRNA sequences to achieve various editing efficiency^{20,23}. Since the quantification of partial gene perturbation by PS is highly accurate (**Fig. 1-2**), we start to investigate whether we can perform dosage-response analysis of perturbation, without the need to titrating the strength of perturbation. By examining ECCITE-seq data that directly measures PDL1 expression (**Fig. 2e**), we found a positive (and negative) correlation between PDL1 expression and the PS score of known PDL1 regulators (**Fig. 3a**). The PS scores of positive PDL1 regulators (e.g., IFNGR1/2, STAT1; **Fig. 3b**) are negatively correlated with PDL1 expression, while the scores of negative regulators (e.g., CUL3, BRD4) show a reverse trend (**Supplementary Fig. S3; Fig. 3c**). For example, CUL3 which is known to destabilize and degrade PDL1 protein expression²⁴. Consequently, higher CUL3 PS scores, indicating higher CUL3 functional perturbation, correspond to higher PDL1 protein expressions (**Fig. 3a**). Compared with mixscape, PS score better predicts the quantitative

changes of PDL1 expression, evidenced by stronger Pearson correlations between the two (**Supplementary Fig. S3**).

We further investigated the relationships between perturbation efficiency and the degree of expression changes, measured by PS score (**Fig. 3d**). In particular, we are interested in genes that show two different patterns of PS scores upon perturbation: “buffered” distribution, where genes have high PS scores only when stronger perturbation efficiency is achieved; and in contrast, “sensitive” distribution, where the PS scores are high, even with moderate or weak perturbation efficiency. CRISPR interference (CRISPRi)-based Perturb-seq datasets are used, as the efficiencies of CRISPR inhibition can be directly evaluated by examining perturbed gene expressions (**Fig. 2e**).

We calculated PS score for every gene in a published essential-wide Perturb-seq²⁵, which uses CRISPRi to inhibit the expressions of 2,285 common essential genes. We classified genes into two different categories (**Fig. 3e**), based on their PS score distributions that correspond to around 50% of perturbation efficiency. Among over 2,000 essential genes, we classified 613 genes as either buffered or sensitive. The majority of these are “buffered” genes (529 out of 613), indicating the robustness of these genes in response to perturbation, possibly due to their essential roles in cellular functions that require compensations on expression reductions. Many “buffered” genes belong to essential protein complex, including proteasomes (e.g., PSMA3; **Fig. 3f**), ribosomal subunit (e.g., RPL4; **Supplementary Fig. S4a**). In contrast, a smaller fraction of “sensitive” genes (185 out of 613) shows strong transcriptome responses even with moderate or weak efficiencies upon perturbing gene expression (**Supplementary Fig. S4b-c**). Notably, 50% reduction of HSPA5 and GATA1 expression achieved near-maximal transcriptional response (and the associated growth defect), which are confirmed by previous studies²⁰.

We further examined possible mechanisms of these “buffered” genes, especially those that belong to the same functional protein complex. Interestingly, perturbing one member of the protein complex usually leads to the expression up-regulation of other members of the complex, indicating a possible mechanism for compensation. For example, perturbing proteasome subunits lead to a strong expression reduction of the perturbed gene (e.g., PSMA5; blue squares in **Fig. 3g**), but at the same time up-regulates other members of the proteasomes (e.g., PSMB7, PSMD2). Perturbing many other protein complexes, including ribosomal subunit, mediator and RNA polymerases, also leads to the similar up-regulation of some members within the same functional unit (**Supplementary Fig. S5a-c**), indicating that compensation occurs by the up-regulation of other subunits of the same molecular machine. To confirm our findings on a different cellular system, we examined the effects from perturbing proteasomes in our genome-scale Perturb-seq dataset (**Fig. 2a**). The TAP-seq approach used in this dataset provides a sensitive and accurate measurement of gene expression changes upon perturbation²¹. Indeed, perturbing members of the proteasome subunits leads to the up-regulation of other proteasomes (**Supplementary Fig. S5d**), consistent with the known transcriptional feedback loop that is observed between proteasome genes²⁶. Overall, the widespread existence of such compensatory effect may explain the perturbation-expression phenotype of buffered genes, where a strong perturbation efficiency is needed to achieve strong expression changes.

PS reveals intrinsic and extrinsic biological factors that regulate gene functions in latent HIV expression.

We next applied our PS model in a Perturb-seq dataset that is designed to investigate the functions of key genes regulating latent HIV-1 expression. We used a Jurkat HIV cell model that we previously

established for pooled CRISPR screening²⁷, where cells stably express Cas9 and are latently infected with HIV-GFP viral vector. We designed Perturb-seq library that targets 10 protein-coding genes (**Supplementary Table S2**), which are either (1) known factors in HIV-1 virus expression and T cell activation (e.g., BIRC2), or (2) top hits from genome-scale CRISPR screens that we previously performed (e.g., BRD4)²⁷. We performed Perturb-seq experiments on three different conditions, including stimulated Jurkat (by PMA/I) followed by GFP expression sorting (GFP+ or GFP-), or unstimulated cells (**Fig. 4a**). The single-cell transcriptomes are profiled via the 10X Genomics Chromium platform, and expressed guide RNAs can be captured directly. After quality controls, we received 7,063-8,811 single cells per sample, where the mean reads per cell (and median genes expressed per cell) in each sample is at least 69,888 (and 4,744), respectively (**Supplementary Fig. S6a**). In terms of guide RNAs, they are detected in over 96% of the cells, and over 85% of these cells can be uniquely assigned a guide RNA (**Supplementary Table S3**). The transcriptome profiles of cells are primarily clustered by cell states (stimulated vs. unstimulated), indicating the primary sources of expression variation is coming from cell states (**Fig. 4b**).

We next investigated gene functions using our PS framework. Among all the perturbed genes, the PS score of BRD4 (bromodomain containing 4) demonstrates a strong cell state-specific pattern, where a subset of cells with BRD4 perturbation has strong BRD4 PS scores (named “BRD4-PS+ cells”) than other BRD4-perturbed cells (or “BRD4-PS- cells; **Fig. 4c**). BRD4-PS+ cells overexpress genes that are involved TNF-alpha signaling, hypoxia and apoptosis (**Fig. 4c-d, Supplementary Fig. S6b-d**). We examined whether the differences in BRD4 PS score reflects the degree of BRD4 functional perturbation. We first checked the expressions of BRD4 “signature” genes from another published study²⁸. Compared with BRD4-PS- cells, BRD4-PS+ cells have a much lower expressions of these signature genes (**Supplementary Fig. S6e**), indicating a stronger functional BRD4 perturbation. In addition, BRD4 is known to inhibit HIV transcription and activation from many studies including our previous CRISPR screens^{27,29}, consistent with the fact that HIV-GFP is one of the top up-regulated genes in BRD4-PS+ cells (**Supplementary Fig. S6f**). Furthermore, BRD4-PS+ cells have a stronger GFP expression (**Fig. 4d**) than other cells, confirming a stronger BRD4 functional perturbation in these cells.

To build a quantitative perturbation-expression relationship, we recalculated BRD4 PS score without using HIV-GFP expression, and examined how the scores are associated with a phenotype of interest (i.e., latent HIV-GFP expression) in different conditions (**Fig. 4e**). BRD4 PS score is correlated with HIV-GFP expression in a cell-state dependent manner: in stimulated T cells (PMA/I treatment), a linear, positive correlation is observed regardless of the GFP expression. In contrast, a nonlinear relationship exists in unstimulated T cells (DMSO), where stronger BRD4 PS score (>0.5) leads to a sharp increase of HIV-GFP expression (**Fig. 4e**).

Another gene, cyclin T1 (CCNT1), also displays heterogeneity in PS score distribution: cells with CCNT1 perturbation have a high PS score distribution only in stimulated cells (**Fig. 4f**). This is different from CCNT1 gene expression or guide distribution, which do not show such pattern differences between cell states (**Supplementary Fig. S7a**). Confirming our findings, the number of DEGs (cells with CCNT1 perturbation vs. cells expressing non-targeting guides) is over one hundred in stimulated cells, where this number is much smaller in non-stimulated cells (adjusted p value <0.001 ; **Supplementary Fig. S7b**). In particular, HIV-GFP is the top DEGs in cells with CCNT1 perturbation, in concordance with the known role of CCNT1 in activating HIV transcription.

CCNT1 is a key subunit of P-TEFb (positive transcription elongation factor b)/CDK9 complex that drives RNA transcription, including the transcription of HIV. The transcription elongation control of P-TEFb/CDK9 is a complicated process that is regulated by multiple mechanisms including various T cell signaling pathways (e.g., NF- κ B signaling), translation control, and epigenetic modification (reviewed in ³⁰). The activities of these factors are different in different states of T cells (e.g., NF- κ B; **Supplementary Fig. S7c**), which may explain the differences of CCNT1 PS scores. Despite the strong cell state dependency of CCNT1 PS score, the quantitative perturbation-expression relationship shows weak correlation within one cell state (**Supplementary Fig. S7d**), which is different from BRD4 PS score (**Fig. 4e**).

To further confirm our finding that different cellular states affect the transcriptomic responses of CCNT1 perturbation, we stimulated Jurkat cells using a different agonist (TNF-alpha). To measure the downstream effect of CCNT1 perturbation, we sorted cells with the expression of HIV-GFP, which is the top down-regulated gene upon CCNT1 knockout (**Supplementary Fig. S7b**), and whose expression is known to be regulated by CCNT1^{31,32}. Indeed, with the presence of TNF-alpha, CCNT1 knockout leads to a strong reduction of HIV-GFP expression (over 50% reduction), while such reduction is much smaller (<5% reduction) in cellular states without TNF-alpha stimulation (**Fig. 4g**). Collectively, these results demonstrated our PS score as a powerful computational framework to investigate cofactors (cell states, other genes) that drive transcriptomic responses upon gene perturbation.

PS identifies novel cell-type dependent gene functions in regulating pancreatic cell differentiation from multiplex single-cell transcriptomics.

Besides Perturb-seq, multiplexing cells with different perturbations are also used to measure single-cell responses of perturbation^{2,18}. A mixture of cells from different perturbations can be sequenced at the same time, and the identity of cells can be established using various methods including cell hashing³³, the expressions of pre-defined barcodes³⁴, or a combination of random barcodes³⁵, etc. We therefore tested our PS framework on pooled single-cell transcriptomics of different perturbations to study the functions of lineage regulators during human pancreatic differentiation. By using an established in vitro human embryonic stem cell (hESC) pancreatic differentiation system, we could generate cells corresponding to early - (definitive endoderm) and middle - (pancreatic progenitor) stages of pancreas development. To test the performance of PS framework and uncover the functions of unknown regulators, we picked ten clonal hESC lines with the homozygous knockout of four genes (**Supplementary Table S4**), including two known pancreatic lineage regulators (HHEX, FOXA1) and two uncharacterized candidate regulators from previous genetic screens (OTUD5, CCDC6)^{36,37}. These clones are then labelled with different LARRY (Lineage and RNA recovery) DNA barcodes³⁴, pooled together and differentiated into definitive endoderm and pancreatic progenitor stages using established protocols³⁶. Finally, the single-cell expressions of these cells are profiled via 10X genomics Chromium platform (**Fig. 5a**). The clone information of each cell is identified from LARRY barcodes. Among 26,286 single cells that passed the quality control measurements, over 97% (25,694/26,286) of the cells have at least one barcode detected, and over 80% (20,678/25,694) are identified as singlets and are retained for downstream analysis. UMAP clustering reveals different known cell types during pancreatic differentiation, based on the expression markers of known cell types (**Fig. 5b; Supplementary Fig. S8**) including definitive endoderm (DE), pancreatic progenitor (PP), liver/duodenum progenitor (LV/DUO), endocrine precursor (EP) as well as cells during the transition stages (e.g., DE in transition, PP in transition).

We next applied our PS framework to the pooled single-cell RNA-seq datasets containing different knockout clones. Among all knockout genes, HHEX PS score is high in cells whose type is between two different differentiated cell types (PP and LP/DP; **Fig. 5c; Supplementary Fig. S8**), in concordance with the known function of HHEX as a key determinant of cell fate decision, whose deletion drives DE cell differentiation towards LP/DP, rather than PP³⁶. Indeed, *HHEX* knockout led to a much fewer percentage of cells that are annotated as PP (**Fig. 5d**). The PS score of FOXA1, another key transcription factor during PP differentiation, is strong in DE and PP cell types, in concordance with the specific expression pattern of FOXA1 in DE/PP cell types (**Supplementary Fig. S9a-c**).

CCDC6 (coiled-coil domain containing 6) is one of the top hits from our previous genome-wide CRISPR screens whose perturbation hinders PP differentiation^{36,38}. However, the exact function of CCDC6 during pancreatic differentiation is largely unknown. We set out to use our PS framework to investigate the functions of CCDC6 at different cell types. Because CCDC6 may have different functions at different cell types, evidenced by the few overlaps of DEG genes between different cell types (**Supplementary Fig. S9d-f**), we calculated PS scores from the DEGs that are performed from four major cell types in the dataset (DE in transition, DE, PP/PP in transition, and LV/DUO). An unbiased clustering on these CCDC6 PS scores demonstrated two distinct cell type-specific distribution patterns (**Fig. 5e**), where scores calculated from later-stage cell types (PP/PP in transition, LV/DUO) are distributed differently from the scores from early-stage cell types (DE in transition, DE; **Fig. 5f**; **Supplementary Fig. S10a-b**), implying different behaviors of CCDC6 perturbation at different cell types. Indeed, functional analysis on DEG genes leading to both patterns have distinct enrichment terms, where in early-stage cell types, DEG genes are enriched in the targets of stem cell transcription factors (e.g., SOX2, POU5F1, NANOG) and cell cycle regulation (**Supplementary Fig. S10c-e**), consistent with the known function of *CCDC6* as a cell cycle regulator^{39,40}. In contrast, DEGs in later-stage cell types are primarily the targets of HNF4A, a key transcription factor that drives LP/DP differentiation (**Fig. 5g; Supplementary Fig. S10f**). The expressions of these transcription factors (SOX2, HNF4A) are among the up-regulated genes in both programs, respectively (**Supplementary Fig. S9d-e**). Furthermore, compared with wild-type cells, *CCDC6* knockout cells have a much fewer percentage of cells that are labelled as PP, and a higher percentage of cells that belong to LP/DP population (**Fig. 5h**). Collectively, these results imply that *CCDC6* play different functions between early or late-stage cell types. Especially in late-stage cell types, *CCDC6* knockout drives cell differentiation towards LV/DUO cell types rather than PP cell types.

To further validate the prediction results of CCDC6, we performed flow cytometry analysis to evaluate the effects of *CCDC6* knockout on the composition of late-stage cell types (PP/LV/DUO). We examined the percentage of HNF4A+ cells, a marker for LV population; and PDX1+ cells, a marker for PP population. Indeed, both clones of *CCDC6* knockout greatly reduced PDX1+ population and increased HNF4A+ population in three biological replicates (**Fig. 5i; Supplementary Fig. S11**), confirming our finding on the enrichment of CCDC6 PS score in LP/DP populations (**Fig. 5f-g**).

Discussion

Understanding cellular responses upon perturbations is a central task in modern biology, from studying tumor heterogeneity to developing personalized medicine. These perturbations may be genetic (e.g., knocking out genes or non-coding elements), chemical (e.g., drug treatments), mechanical (e.g., pressure) or environmental (e.g., temperature changes). Single-cell genomics profiles of perturbations is a common technique to investigate the mechanisms of perturbations. Many technologies, including

Perturb-seq and sci-Plex, enable a high-content readout of systematically perturbing many genes or non-coding elements. Despite the rapid advancements of technology, a major bottleneck is that we lack a computational model to fully unlock the potential of high-content perturbation, especially on discovering novel biological insights from the data. Here we introduce a Perturbation Score (PS) framework to model the heterogenous transcriptomic responses of perturbations and to enable novel biological discovery from modeling perturbation heterogeneity.

Partial gene perturbation is common in perturbation experiments. Partial perturbations may come from dose-controlled drug treatment, the gene editing technology that does not fully knockout gene function (e.g., RNA- or CRISPR-interference, epigenome editors), or from CRISPR/Cas9 that generate random DNA editing outcomes. We demonstrated the outstanding performance of our PS method over existing methods in quantifying partial gene perturbation. Especially, such partial perturbation identification enables the analysis of dosage-dependent effect, which is demonstrated in this study using various datasets.

More importantly, PS enables novel biological knowledge discovery including (1) dosage analysis of perturbation without the need to titrate perturbation strength, and (2) identification of biological factors, both intrinsic or extrinsic, that regulate perturbation responses. In this case, the PS score, ranging between 0 and 1, no longer represents the quantity of partial perturbation, but instead represents the strength of the perturbation outcome. In the latter case, PS becomes a convenient tool to identify cell context that determines perturbation outcome. We demonstrated the application of PS in various biological problems, including T cell activation, essential gene function, latent HIV-1 virus expression and pancreatic cell differentiation. Importantly, our PS model leads the discovery of novel CCDC6 functions that are cell type dependent, whose role as a regulator during pancreatic and liver cell fate decision is experimentally validated.

Partial perturbations of gene functions contribute to the complexity of many biological processes. For example, “haploinsufficient” genes are able to cause disease phenotypes when 50% of their functions are disrupted, while “haplosufficient” genes will require a nearly complete gene knockout. However, we currently lack a method to investigate the phenotypes of partial gene perturbations, and to efficiently perform dosage analysis at a large scale. Current approaches, e.g., by introducing mismatches to guide RNAs to modulate the effects of CRISPR inhibitions (CRISPRi)²⁰ or Cas13¹³, require a complex design of a specific CRISPR system. Here we demonstrated that both CRISPR knockout and CRISPRi naturally introduce partial perturbation effects, which can be used to study the dosage effect of partial gene perturbations on affecting downstream gene expressions or a phenotype of interest. Our PS framework is versatile, enabling the dosage analysis using various perturbation methods (e.g., CRISPRi or CRISPR knockout) and assays (e.g., Perturb-seq or multiplex scRNA-seq).

Results from genetic perturbations (e.g., via CRISPR/Cas9) are informative for drug development, and confirmations from genetic perturbation experiments are usually required to demonstrate the feasibility of candidate drug targets. However, titrating pharmaceutical interventions are easy (e.g., by using different doses of drugs), while it is much more difficult to precisely control the degree of genetic perturbations. Our PS framework provides a convenient alternative to dosage-dependent perturbations, especially genetic perturbations, and their associations with phenotypic changes, which will be informative in designing drugs. For example, BRD4 is the primary target of bromodomain inhibitors (BETi), many of which have been proposed as candidates of latency reversing agents (LRAs) to

reactivate latent HIV-1 expression. The distribution of BRD4 PS scores (**Fig. 3**) reveals that stronger perturbation effects are needed to induce the desired phenotype, in this case, the expression of HIV-GFP (**Fig. 3**). Since BRD4 is an essential gene, a strong BRD4 perturbation may lead to unexpected toxicity, thereby limiting the efficacy of BETi. Indeed, our previous study²⁷ demonstrated that 10-1000x higher doses of JQ1, a commonly used BETi, are needed to induce latent HIV-1 expression at a similar level with other potent LRAs. Our results further warrant the development of synergistic drug combinations to mitigate the narrow therapeutic window of BETi, which is currently tested in many studies.

Methods

The Perturbation Score (PS) framework

The estimation of PS consists of three steps, as are illustrated in Figure 1c: target gene identification (Step 1), average perturbation effect estimation using a previously published scMAGECK (Step 2), and PS estimation using constrained optimization (Step 3).

Step 1: target gene identification. We first performed differential expression analysis between cells with certain perturbation (e.g., knocking out gene X) and negative control cells. In most cases, negative control cells are cells that express non-targeting guide RNAs (in Perturb-seq), or wild-type cells (in pooled scRNA-seq). In Perturb-seq that is performed with high MOI condition, these cells may come from cells that do not have a particular perturbation. We used Wilcoxon Rank Sum test (implemented in Seurat) to identify and rank differentially expressed genes. Top genes are then selected as potential target genes of the specific perturbation. The maximum and minimum numbers of top genes can be specified by the user. Alternatively, users can also provide the list of target genes of that perturbation, based on the prior knowledge, therefore skipping the differential expression analysis in this step.

Step 2: average perturbation effect estimation. We used the linear regression module in scMAGECK (scMAGECK-LR) to estimate the average perturbation effect. scMAGECK-LR takes the expressions of all target genes (identified in Step 1) in all cells as input, and outputs a “ β ” score, a score that is conceptually similar with log fold change. The advantages of using β score, instead of simply using the log fold changes in Step 1, are twofold. First, scMAGECK-LR naturally supports datasets from high MOI Perturb-seq, where one cell may express multiple guides targeting different genes. Second, scMAGECK-LR is able to estimate average perturbation effects of multiple perturbations (e.g., genome-scale perturbations) in one step, while a naïve DEG analysis can only calculate LFC for each perturbation.

The mathematical model of scMAGECK-LR is described as follows. Let Y be the log-transformed, $M \times N$ expression matrix of M single cells and N target genes. These genes are the union of all target genes for all K perturbations, extracted from Step 1. Let D be the $M \times K$ binary cell identity matrix of M single cells and K perturbations, where $d_{jX} = 1$ if single cell j contains sgRNAs targeting gene X ($j = 1, 2, \dots, M; X = 1, 2, \dots, K$), and $d_{jX} = 0$ otherwise. D can be obtained from the detected guide RNA expression matrix from Perturb-seq, or from the prior sample information from pooled scRNA-seq. The effect of target gene knockout on all expressed genes is indicated as a β score in a matrix B with size $K \times N$, where $\beta_{XA} > 0$ (< 0) indicates gene X is positively (or negatively) selected on gene A expression, respectively. In other words, gene X knockout increases (or decreases) gene A expression if $\beta_{XA} > 0$ (< 0), respectively.

The log-transformed expression matrix Y is modeled as follows:

$$Y = Y_0 + D \times B + \epsilon \quad \text{Eq (1)}$$

Where Y_0 is the basal expression level of all genes in an unperturbed state, ϵ is a noise term following a Gaussian distribution with zero means. Y_0 can be estimated from negative control cells (e.g., wild-type cells or cells expressing non-targeting guides), or be modeled using the expressions of neighboring negative control cells (e.g., the approach used by mixscape¹⁶). The value of B can be estimated using ridge regression:

$$B = (D^T D + \lambda I)^{-1} D^T Y \quad \text{Eq (2)}$$

where I is the identity matrix, and λ is a small positive value (default 0.01).

Step 3: PS estimation using constrained optimization. We revise Eq (1) to incorporate PS score. Here, the log-transformed expression matrix Y is modelled as follows:

$$Y = Y_0 + \Psi \times B + \epsilon \quad \text{Eq (3)}$$

Where Ψ is the non-negative, raw PS score matrix with the same size as D in Step 2 ($M \times K$). Each element ψ_{jx} in Ψ indicates the raw PS score of cell j of perturbing gene X . Here, B is the β score matrix which is estimated in Step 2. We find the value of Ψ to minimize the squared error of predicted and observed expressions of all genes within all cells, subject to constraints and regularization terms:

$$\min \sum_{ji} (y_{ji} - y_{ji}^0 - \sum_k \psi_{jk} \beta_{ki})^2 + \lambda \sum_{jk} |\psi_{jk}| \quad \text{Eq (4)}$$

subject to the following constraints:

$$\begin{cases} 0 \leq \psi_{jk} \leq U, & \text{if } d_{jk} = 1 \\ \psi_{jk} = 0 & \text{if } d_{jk} = 0 \end{cases}$$

Here, U is a positive value indicating the upper bound of raw Ψ values, and d_{ik} is the value of the binary cell identity matrix in Step 2. $1 \leq j \leq M$ is the index of single cells, $1 \leq i \leq N$ is the index of target genes, and $1 \leq k \leq K$ is the index of perturbations.

Because we are imposing non-negative constraints to Ψ , the absolute operator can be removed from the objective function in Eq (4) and can be rewritten as:

$$\min \sum_{ji} (y_{ji} - y_{ji}^0 - \sum_k \psi_{jk} \beta_{ki})^2 + \lambda \sum_{jk} \psi_{jk} \quad \text{Eq (4)}$$

This becomes a constrained quadratic optimization problem where the best solution can be easily achieved using methods like Newton's method. The final, normalized PS score is to scale values of ψ_{ik} to $[0,1]$:

$$PS_{ik} = \psi_{ik} / U$$

We implemented this framework as part of scMAGeCK pipeline¹⁵ (<https://github.com/weililab/scMAGeCK>).

Simulated datasets

Genome-scale Perturb-seq on Jurkat cells

Perturb-seq. We performed genome-scale Perturb-seq on Jurkat E6 cell line expressing dCas9-KRAB as our model to study. We transduced them with a genome-wide CRISPRi CROP-seq library at a high multiplicity of infection (MOI). After infection, we split the cells into two populations, including untreated cells and activated cells (cells treated with anti-TCR and anti-CD28 antibodies for approximately 24 hours to stimulate TCR signaling). Cells were then labelled with cell hashing antibodies. Multiple labels were used for the activated population to help with cell multiplet detection. Cells were loaded on 16 channels of a 10x Chromium X instrument. We loaded 115000 cells per channel, and the expected recovery rate is 60 000 cells per channel, including 24% multiplets. Samples were pooled unequally before they were loaded on the ChromiumX: 10% untreated cells, 90% treated cells. Sequencing library was prepared using 3'Chemistry with a targeted primer panel, i.e. custom multiplex PCR step to enrich for specific transcripts. Libraries were sequenced on NovaSeq S4 PE100 in asymmetric read mode (R1: 28 cycles; R2: 172 cycles), with PhiX concentration of 1%. The expected coverage is around 9 000 ~ 10 000 input reads per cell.

Hash oligos.

oligo	condition
CGGCTCGTGTGCGTCGTCTCAAGTCCAGAAACTCCGTGTATCCT	untreated
CTCCCTGGTGTTCATAACCCGATGTGGTGGGCAGAATGTGGCTGG	activated
TTACCCGCAGGAAGACGTATAACCCCTCGTGCCAGGCGACCAATGC	activated
TGTCTACGTGGACCGCAAGAAGTGGAGTCAGAGGCTGCACGCTGT	activated
CCCCACCAGGTTGCTTGTGGACGAGCCCGCACAGCGCTAGGAT	activated
GTGATCCCGCGCAGGCACACATACCGACTCAGATGGGTTGTCCAGG	activated
GCAGCCGGCGTCGTACGAGGCACAGCGGAGACTAGATGAGGCCCG	activated

sgRNA library design. Genome-wide CRISPRi sgRNA library was designed to target the transcription start site (TSS) coordinates, calculated from publicly available FANTOM CAGE peaks data. In total 18 595 genes are targeted with 4 sgRNAs per gene. On top of that, we designed another CRISPRi library targeting 3220 genes with 4 sgRNAs per gene. This library was designed using Jurkat-specific TSS which were calculated from public Jurkat CAGE-seq datasets. Both libraries were combined into a final library targeting 3220 genes with 8 sgRNA/gene and 15 375 genes with 4 sgRNA/gene.

Targeted primer panel. The primer panel for targeted transcriptomic readout consists of 374 target genes from several categories:

Source	Number of targets (genes)
bulk RNA-seq DEG, 50 top up/downregulated	100
T-cell related genes	51
KEGG TCR signaling pathway	35
RNA-binding proteins	27
Replogle*: unfolded protein response	51
Replogle: proteasome	41
Replogle: NFkB	20
Replogle: cell cycle	29

Replogle: targets of nonsense-mediated decay	5
Controls (cell cycle, mitochondrial, Cas9)	15
Total number of targets	374

* “Replogle” prefix means that this category of targets was derived from the published genome-scale Perturb-seq dataset²⁵.

Data preprocessing. For each of the 16 channels, all 3 kinds of sequencing libraries (mRNA, sgRNA, cell hashing) are indexed using the same Illumina index sequence. We obtained high-quality scRNA-seq data of over 586,000 single cells after quality control, with a median 13 guides detected per cell. We obtained an average of 400 cells per gene perturbation. STAR and STAR solo 2.7.10a was used to map transcriptomic reads against a custom gtf annotation which was based on gencode.v34.annotation.gtf (hg38). Reads that did not map to the transcriptome reference were then mapped & counted using STAR solo against a custom fasta reference with guide sequences and a fasta reference with hash label sequences. STAR Solo output transcriptome matrices are first filtered using an approach similar to 10x cellranger EmptyDrops filtering, which retained cells with at least 10 % UMI count of the 99th percentile UMI counts of top expected cells number. Then, initial Seurat object was created from those filtered transcriptome matrices using CreateSeuratObject function with following parameters: min.cells = 5 , min.features = 10 , all other parameters are left with default values. Outlier cells were filtered out by mitochondrial and mRNA content (percent.mt , nCount_RNA). In order to detect cell multiplets and determine cell population (untreated or activated), cell labels (also known as hashes) are called using MULTI-seq approach (deMULTIplex::classifyCells in R). Only cells with exactly 1 known label are kept. Then, sgRNA calling was done using binomial test with total sgRNA UMI counts used to derive background frequencies. A threshold of 0.05 on Benjamini Hochberg corrected p-values (per channel) was used to generate the final calls. The sgRNA assays are sparse matrices containing 1 where the respective cell is considered as carrying the respective sgRNA and 0 elsewhere. Following that, all results from steps above from 16 channels are merged together, and merged counts are normalized using NormalizeData and scaled using ScaleData cell cycle scoring is performed via CellCycleScoring, PCA is calculated using RunPCA and UMAP is calculated on first 30 principal components using RunUMAP in Seurat.

HIV latency Perturb-seq

We used a previously established cell line model of HIV latency²⁷. In this model, Jurkat cells were infected with an HIV vector with GFP tied to the LTR promoter, resulting in a positive GFP signal as a measurement of viral transcription reactivation and HIV latency reversal. These cells, which already express Cas9, were transduced with a lenti-sgRNA library. The lenti-sgRNA library (MilliporeSigma; LV14, U6-gRNA-10x:EF1a-Puro-2a-BFP) was designed to target 10 genes with 3 gRNAs per gene. In addition to non-targeting controls, the library contained five positive regulators (NFKB1, CCNT1, PRKCA, TLR1, MAP3K14) and five negative regulators (NFKBIA, NELFE, HDAC2, BRD4, BIRC2) of HIV transcription. Transduction was carried out on 850,000 cells at an MOI of 0.3 using 8ug/ml polybrene in 2 ml of RPMI containing 10% FBS and 1% penicillin–streptomycin. The media was replaced 24 hours later with fresh media without polybrene. Two days after transduction, the cells were selected for using 1.5 ug/ml puromycin for 5 days. After selection, the cells were split evenly into three groups. One third of the cells were kept in culture with no drug added, while two thirds of the cells were stimulated with PMA/I (50ng/ml PMA in combination with 1 μ M Ionomycin). After 16 hours, the

stimulated cells were sorted into GFP+ and GFP- populations. All three groups were then analyzed following the 10x Genomics single-cell sequencing protocol.

Pancreatic differentiation clones and pooled single-cell RNA-seq

Culture of hESC. The generation of KO hESCs were described in published studies, including HHEX KO H1 and HUES8 cell lines³⁶, FOXA1 KO HUES8 cell lines⁴¹, OTUD5 KO HUES8 cell lines and CCDC6 KO H1 cell lines³⁷. Cells were regularly confirmed to be mycoplasma-free by the Memorial Sloan Kettering Cancer Center (MSKCC) Antibody & Bioresource Core Facility. KO and WT hESCs were maintained in Essential 8 (E8) medium (Thermo Fisher Scientific, A1517001) on vitronectin (Thermo Fisher Scientific, A14700) pre-coated plates at 37°C with 5% CO₂. The Rho-associated protein kinase (ROCK) inhibitor Y-276325 (5μM; Selleck Chemicals, S1049) was added to the E8 medium the first day after passaging or thawing of hESCs.

hESC-directed pancreatic differentiation. hESCs were seeded at a density of 2.3×10^5 cells/cm² on vitronectin-coated plates in E8 medium with 10μM Y-27632. After 24 hours, cells were washed with PBS and differentiated to DE (stage 1), primitive gut tube (stage 2), PP1 (stage 3) and PP2 (stage 4) stages following previously described 4-stage protocol³⁶. In brief, stage 1 (3 d): S1/2 medium supplemented with 100ng ml⁻¹ Activin A (Bon Opus Biosciences) and 5μM CHIR99021 (04-0004-10, Stemgent) for 1 d. S1/2 medium supplemented with 100ng ml⁻¹ Activin A for the next 2 d. Stage 2 (2 d): S1/2 medium supplemented with 50ng ml⁻¹ KGF (AF-100-19, PeproTech) and 0.25mM vitamin C (VitC) (Sigma-Aldrich, A4544). Stage 3 (2 d): S3/4 medium supplemented with 50ng ml⁻¹ KGF, 0.25mM VitC and 1μM retinoic acid (R2625, MilliporeSigma). Stage 4 (4 d): S3/4 medium supplemented with 50ng ml⁻¹ KGF, 0.1μM retinoic acid, 200nM LDN (Stemgent, 04-0019), 0.25μM SANT-1 (Sigma, S4572), 0.25mM VitC and 200nM TPB (EMD Millipore, 565740). The base differentiation medium formulations used in each stage were as follows. S1/2 medium: 500ml MCDB 131 (15-100-CV, Cellgro) supplemented with 2 ml 45% glucose (G7528, MilliporeSigma), 0.75g sodium bicarbonate (S5761, MilliporeSigma), 2.5g BSA (68700, Proliant), 5ml GlutaMAX (35050079, Invitrogen). S3/4 medium: 500ml MCDB 131 supplemented with 0.52ml 45% glucose, 0.875g sodium bicarbonate, 10g BSA, 2.5ml ITS-X, 5ml GlutaMAX.

Cell infection with LARRY barcode virus. Individual LARRY barcode constructs were cloned from LARRY barcode library (Addgene:140024) and transfected to 293T cells to generate lentivirus. Next, each KO and WT hESC clone was infected with a unique LARRY barcode at low MOI. One week after lentiviral infection, the barcoded cells, which expressed GFP, were sorted out and cultured in E8 medium as described in previous section.

Pooled single-cell RNA-seq. One day before differentiation, each of 10 hESC barcoded clones were counted, mixed at the same cell number ratio and then seeded at a density of 2.3×10^5 cells/cm² onto 12-well cell culture plate. At DE and PP2 stages, pooled differentiating cells were dissociated into single cell suspension by TrypLE Select for 5min at 37°C. Cells were then stored in BAMBANKER™ freezing medium for future experiments. For scRNA-seq, frozen cells were thawed and sorted to collect live GFP+ cells. Cellular suspensions were then loaded on a Chromium Controller following the manufacturer's instructions (10x Genomics Chromium Single Cell 3' Reagent Kit v3.1 User Guide). cDNA libraries and targeted LARRY barcode libraries were generated separately using 10ul cDNA each. cDNA libraries were made under manufacturer's instructions and targeted LARRY barcode libraries

were amplified using specific primers (F: CTACACGACGCTCTCCGATCT; R: GTGACTGGAGTTCAGACGTGTGCTCTCCGATCTtaaccgttgcttaggagagaccataT).

Flow cytometry. Cells were dissociated using TrypLE Select and resuspended in FACS buffer (5% FBS in PBS). Live-Dead Fixable Violet Dead cell stain (Invitrogen, L34955) was used to discriminate dead cells from live cells. Permeabilization/fixation was performed at room temperature for 1 h. Antibody staining was performed in permeabilization buffer. Antibodies for this study include: HNF4A, Novus Biologicals, NBP2-67679, 1:200; PDX1, R&D Systems, AF2419, 1:500, Donkey anti-Rabbit IgG (H+L) Highly Cross-Adsorbed Secondary Antibody, Thermo Fisher Scientific, 1:500; Donkey anti-goat IgG (H+L) Highly Cross-Adsorbed Secondary Antibody, Thermo Fisher Scientific, 1:500. Cells were then analysed using BD LSRFortessa. Flow cytometry analysis and figures were generated using FlowJo v.10.

Acknowledgements

The authors thank all members from the Li and Huangfu laboratory for comments and discussions. The authors thank Jake P. Taylor-King for discussions. This study is supported from NIH R01 HG010753, HL168174 (to W.L., B.S., L.C.), District of Columbia Center for AIDS (DC-CFAR) Research Transitioning Investigator Award (AI117970, to W.L.), and startup support from the Center for Genetic Medicine Research at Children's National Hospital. D.H is supported by NIH (UM1HG012654, U01HG012051). J.J. Li is supported by National Science Foundation DBI-1846216 and DMS-2113754, NIH/NIGMS R35GM140888, Johnson and Johnson WiSTEM2D Award, Sloan Research Fellowship, UCLA David Geffen School of Medicine W.M. Keck Foundation Junior Faculty Award, and Chan-Zuckerberg Initiative Single-Cell Biology Data Insights [Silicon Valley Community Foundation Grant Number: 2022-249355]. W.D. and R.F.S. is supported by the Howard Hughes Medical Institute.

Author contributions

W.L. conceived the project. W.L. and B.S. developed the method. W.L., B.S., and D.L. designed and performed the experiments and analyzed the data. W.D., N.M. and B.S. performed and analyzed HIV Perturb-seq under the supervision of J.M.S., R.S. and W.L. B.S., Q.W. and D.S. performed synthetic experiments under the supervision of W.L. and J.J.L. D.L., D.Y., B.W. and B.R. generated pancreatic differentiation dataset and performed validations under the supervision of D.H. A.K., A.V., N.U., and A.L. generated and analyzed genome-scale Perturb-seq under the supervision of T.B. X.C., L.C. and Y.D. performed the analysis and interpretation of the results. W.L., and B.S. wrote the manuscript with input from all the authors. W.L. T.B., J.J.L., R.S. and D.H. supervised the study.

Competing interests

T.B. is a co-founder and Managing Director of Myllia Biotechnology. A.K., A.V., N.U. and A.L. are employees of Myllia Biotechnology. Other authors declare that they have no competing interest.

Data and materials availability

The genome-scale T-cell Perturb-seq, HIV Perturb-seq, and pancreatic scRNA-seq data have been deposited to Gene Expression Omnibus (GEO) and Short Read Archive (SRA). The source code of the PS method is available as part of scMAGeCK pipeline¹⁵ on GitHub: (<https://github.com/weililab/scMAGeCK>).

References

- 1 High-content CRISPR screening. *Nat Rev Methods Primers* 2022;2:.. <https://doi.org/10.1038/s43586-022-00098-7>.
- 2 Srivatsan SR, McFaline-Figueroa JL, Ramani V, Saunders L, Cao J, Packer J, *et al.* Massively multiplex chemical transcriptomics at single-cell resolution. *Science* 2020;367:45–51.
- 3 Dixit A, Parnas O, Li B, Chen J, Fulco CP, Jerby-Arnon L, *et al.* Perturb-Seq: Dissecting Molecular Circuits with Scalable Single-Cell RNA Profiling of Pooled Genetic Screens. *Cell* 2016;167:1853-1866.e17.
- 4 Adamson B, Norman TM, Jost M, Cho MY, Nuñez JK, Chen Y, *et al.* A Multiplexed Single-Cell CRISPR Screening Platform Enables Systematic Dissection of the Unfolded Protein Response. *Cell* 2016;167:1867-1882.e21.
- 5 Jaitin DA, Weiner A, Yofe I, Lara-Astiaso D, Keren-Shaul H, David E, *et al.* Dissecting Immune Circuits by Linking CRISPR-Pooled Screens with Single-Cell RNA-Seq. *Cell* 2016;167:1883-1896.e15.
- 6 Datlinger P, Rendeiro AF, Schmidl C, Krausgruber T, Traxler P, Klughammer J, *et al.* Pooled CRISPR screening with single-cell transcriptome readout. *Nat Methods* 2017;14:297–301.
- 7 Xie S, Duan J, Li B, Zhou P, Hon GC. Multiplexed Engineering and Analysis of Combinatorial Enhancer Activity in Single Cells. *Mol Cell* 2017;66:285-299.e5.
- 8 Rubin AJ, Parker KR, Satpathy AT, Qi Y, Wu B, Ong AJ, *et al.* Coupled Single-Cell CRISPR Screening and Epigenomic Profiling Reveals Causal Gene Regulatory Networks. *Cell* 2019;176:361-376.e17.
- 9 Liscovitch-Brauer N, Montalbano A, Deng J, Méndez-Mancilla A, Wessels H-H, Moss NG, *et al.* Profiling the genetic determinants of chromatin accessibility with scalable single-cell CRISPR screens. *Nat Biotechnol* 2021;39:1270–7.
- 10 Dhainaut M, Rose SA, Akturk G, Wroblewska A, Nielsen SR, Park ES, *et al.* Spatial CRISPR genomics identifies regulators of the tumor microenvironment. *Cell* 2022;185:1223-1239.e20.
- 11 Norman TM, Horlbeck MA, Replogle JM, Ge AY, Xu A, Jost M, *et al.* Exploring genetic interaction manifolds constructed from rich single-cell phenotypes. *Science* 2019;365:786–93.
- 12 Replogle JM, Norman TM, Xu A, Hussmann JA, Chen J, Cogan JZ, *et al.* Combinatorial single-cell CRISPR screens by direct guide RNA capture and targeted sequencing. *Nat Biotechnol* 2020;38:954–61.
- 13 Wessels H-H, Méndez-Mancilla A, Hao Y, Papalexi E, Mauck WM 3rd, Lu L, *et al.* Efficient combinatorial targeting of RNA transcripts in single cells with Cas13 RNA Perturb-seq. *Nat Methods* 2023;20:86–94.
- 14 Hill AJ, McFaline-Figueroa JL, Starita LM, Gasperini MJ, Matreyek KA, Packer J, *et al.* On the design of CRISPR-based single-cell molecular screens. *Nat Methods* 2018;15:271–4.
- 15 Yang L, Zhu Y, Yu H, Cheng X, Chen S, Chu Y, *et al.* scMAGECK links genotypes with multiple phenotypes in single-cell CRISPR screens. *Genome Biol* 2020;21:19.
- 16 Papalexi E, Mimitou EP, Butler AW, Foster S, Bracken B, Mauck WM 3rd, *et al.* Characterizing the molecular regulation of inhibitory immune checkpoints with multimodal single-cell screens. *Nat Genet* 2021;53:322–31.

17 Song D, Wang Q, Yan G, Liu T, Sun T, Li JJ. scDesign3 generates realistic in silico data for multimodal single-cell and spatial omics. *Nat Biotechnol* 2023. <https://doi.org/10.1038/s41587-023-01772-1>.

18 Wu B, Zhang X, Chiang H-C, Pan H, Yuan B, Mitra P, *et al.* RNA polymerase II pausing factor NELF in CD8+ T cells promotes antitumor immunity. *Nat Commun* 2022;13:2155.

19 Gasperini M, Hill AJ, McFaline-Figueroa JL, Martin B, Kim S, Zhang MD, *et al.* A Genome-wide Framework for Mapping Gene Regulation via Cellular Genetic Screens. *Cell* 2019;176:1516.

20 Jost M, Santos DA, Saunders RA, Horlbeck MA, Hawkins JS, Scaria SM, *et al.* Titrating gene expression using libraries of systematically attenuated CRISPR guide RNAs. *Nat Biotechnol* 2020;38:355–64.

21 Schraivogel D, Gschwind AR, Milbank JH, Leonce DR, Jakob P, Mathur L, *et al.* Targeted Perturb-seq enables genome-scale genetic screens in single cells. *Nat Methods* 2020;17:629–35.

22 Shifrut E, Carnevale J, Tobin V, Roth TL, Woo JM, Bui CT, *et al.* Genome-wide CRISPR screens in primary human T cells reveal key regulators of immune function. *Cell* 2018;175:1958–1971.e15.

23 Wessels H-H, Stirn A, Méndez-Mancilla A, Kim EJ, Hart SK, Knowles DA, *et al.* Prediction of on-target and off-target activity of CRISPR-Cas13d guide RNAs using deep learning. *Nat Biotechnol* 2023. <https://doi.org/10.1038/s41587-023-01830-8>.

24 Zhang J, Bu X, Wang H, Zhu Y, Geng Y, Nihira NT, *et al.* Cyclin D–CDK4 kinase destabilizes PD-L1 via cullin 3–SPOP to control cancer immune surveillance. *Nature* 2018;553:91–5.

25 Replogle JM, Saunders RA, Pogson AN, Hussmann JA, Lenail A, Guna A, *et al.* Mapping information-rich genotype-phenotype landscapes with genome-scale Perturb-seq. *Cell* 2022;185:2559–2575.e28.

26 Radhakrishnan SK, Lee CS, Young P, Beskow A, Chan JY, Deshaies RJ. Transcription factor Nrf1 mediates the proteasome recovery pathway after proteasome inhibition in mammalian cells. *Mol Cell* 2010;38:17–28.

27 Dai W, Wu F, McMyn N, Song B, Walker-Sperling VE, Varriale J, *et al.* Genome-wide CRISPR screens identify combinations of candidate latency reversing agents for targeting the latent HIV-1 reservoir. *Sci Transl Med* 2022;14:eaah3351.

28 Shu S, Wu H-J, Ge JY, Zeid R, Harris IS, Jovanović B, *et al.* Synthetic Lethal and Resistance Interactions with BET Bromodomain Inhibitors in Triple-Negative Breast Cancer. *Mol Cell* 2020;78:1096–1113.e8.

29 Li Z, Guo J, Wu Y, Zhou Q. The BET bromodomain inhibitor JQ1 activates HIV latency through antagonizing Brd4 inhibition of Tat-transactivation. *Nucleic Acids Res* 2013;41:277–87.

30 Mbonye U, Kizito F, Karn J. New insights into transcription elongation control of HIV-1 latency and rebound. *Trends Immunol* 2023;44:60–71.

31 Wei P, Garber ME, Fang S-M, Fischer WH, Jones KA. A novel CDK9-associated C-type cyclin interacts directly with HIV-1 tat and mediates its high-affinity, loop-specific binding to TAR RNA. *Cell* 1998;92:451–62.

32 Peng J, Zhu Y, Milton JT, Price DH. Identification of multiple cyclin subunits of human P-TEFb. *Genes Dev* 1998;12:755–62.

33 Stoeckius M, Zheng S, Houck-Loomis B, Hao S, Yeung BZ, Mauck WM 3rd, *et al.* Cell Hashing with barcoded antibodies enables multiplexing and doublet detection for single cell genomics. *Genome Biol* 2018;19:224.

34 Weinreb C, Rodriguez-Fraticelli A, Camargo FD, Klein AM. Lineage tracing on transcriptional landscapes links state to fate during differentiation. *Science* 2020;367:eaaw3381.

35 Vitak SA, Torkency KA, Rosenkrantz JL, Fields AJ, Christiansen L, Wong MH, *et al.* Sequencing thousands of single-cell genomes with combinatorial indexing. *Nat Methods* 2017;14:302–8.

36 Yang D, Cho H, Tayyebi Z, Shukla A, Luo R, Dixon G, *et al.* CRISPR screening uncovers a central requirement for HHEX in pancreatic lineage commitment and plasticity restriction. *Nat Cell Biol* 2022;24:1064–76.

37 Rosen BP, Li QV, Cho H, Liu D, Yang D, Graff S, *et al.* Parallel genome-scale CRISPR screens distinguish pluripotency and self-renewal. *BioRxiv.org* 2023. <https://doi.org/10.1101/2023.05.03.539283>.

38 Li QV, Dixon G, Verma N, Rosen BP, Gordillo M, Luo R, *et al.* Genome-scale screens identify JNK-JUN signaling as a barrier for pluripotency exit and endoderm differentiation. *Nat Genet* 2019;51:999–1010.

39 Thanasopoulou A, Stravopodis DJ, Dimas KS, Schwaller J, Anastasiadou E. Loss of CCDC6 affects cell cycle through impaired intra-S-phase checkpoint control. *PLoS One* 2012;7:e31007.

40 Morra F, Luise C, Merolla F, Poser I, Visconti R, Ilardi G, *et al.* FBXW7 and USP7 regulate CCDC6 turnover during the cell cycle and affect cancer drugs susceptibility in NSCLC. *Oncotarget* 2015;6:12697–709.

41 Lee K, Cho H, Rickert RW, Li QV, Pulecio J, Leslie CS, *et al.* FOXA2 is required for enhancer priming during pancreatic differentiation. *Cell Rep* 2019;28:382–393.e7.

Figure Legends

Figure 1. The Perturbation Score (PS) framework and benchmark. **a**, Overview of different technical and biological factors that contribute to heterogenous perturbation outcomes from single-cell perturbation datasets. **b**, Using downstream gene expressions to infer the value of PS scores. **c**, Overview of the scMAGECK-PS that estimates PS value. **d-e**, Benchmark results of both PS and mixscape using simulated datasets, where 50% (**d**) and 100% (**e**) gene perturbation effects are simulated using scDesign3. Here, the expressions of 200 differentially expressed genes (DEGs) from bulk RNA-seq (Nelf knockout vs. wild-type) are simulated, and ground truth efficiency value is indicated in red color. **f**, Benchmark pipeline using real CRISPR interference (CRISPRi)- based Perturb-seq datasets, where the perturbation efficiency can be evaluated directly via gene expression. **g-h**, Benchmark results of mixscape and scMAGECK-PS using a published Perturb-seq dataset, by counting the numbers of cells or genes with strong perturbation effects. A gene is considered to have strong perturbation effect, if a strong negative correlation (Pearson correlation coefficient < -0.1) is observed between the perturbation score and the expression of that gene across all perturbed cells. A cell is considered to be strongly perturbed, if its predicted efficiency score (by scMAGECK-PS or mixscape) within one cell is greater than 0.5. The Perturb-seq experiment is performed with low MOI condition, where most cells have only 1 expressed guide. **i**, An representative estimation results of scMAGECK-PS and their correlations of ACTB expression.

Figure 2. Additional benchmark results using genome-scale Perturb-seq and ECCITE-seq. **a**, Benchmark procedure using a genome-scale Perturb-seq and a published, pooled T cell CRISPR screen. **b**, The distribution of unstimulated and stimulated Jurkat cells along the UMAP plot. **c**, The correlation of predicted scores by scMAGECK-PS and mixscape. **d**, the Receiver-Operating Characteristic (ROC)

curve of both methods in separating positive and negative hits. **e-f**, Benchmark using a published ECCITE-seq where PDL1 protein expression is used as gold standard (**e**), and the performance of different methods in terms of predicting PDL1 protein expression (**f**).

Figure 3. Dosage-dependent responses of perturbations. **a**, The correlation between a gene's PS score and a phenotype of interest indicates positive (or negative) regulations. **b-c**, The correlation between PDL1 protein expression and the PS score of CUL3 (**b**) and STAT1 (**c**). CUL3 is a known negative regulator of PDL1, while STAT1 is a known positive regulator. **d**, The classification of buffered or sensitive genes, based on perturbed gene expression and PS score. **e**, The classification of buffered or sensitive genes from published Perturb-seq datasets focusing essential genes in K562²⁵. **f**, The perturbation-expression plot of PSMA3, a buffered gene. **g**, The log fold changes of mark gene expressions (columns) upon perturbing proteasome genes (rows) from the essential gene Perturb-seq dataset.

Figure 4. Perturb-seq on HIV latency. **a**, The experimental design of Perturb-seq. **b**, The UMAP plot of single-cell transcriptome profiles. Cells are colored by three different conditions. **c**, The distribution of BRD4 PS score. **d**, The expression of HIV-GFP. **e**, The correlations between HIV-GFP expression and BRD4 PS score that does not use HIV-GFP as target gene. **f**, The distribution of CCNT1 PS score. **g**, The protein expression of HIV-GFP in response to CCNT1 knockout in different cell states (TNF-alpha vs non-stimulated).

Figure 5. Pooled scRNA-seq on pancreatic differentiation. **a**, Experimental design of multiplexing scRNA-seq on the knockout clones of different genes. **b**, The UMAP plot of single-cell transcriptome profiles, colored by different clusters (left) or clones (right). **c**, The PS score distribution of HHEX. **d**, The percentage of cells in PP/LV/DUO cell types from different clones. **e**, The correlations of CCDC6 PS scores calculated from different HHEX cell types. The Pearson Correlation Coefficient (PCC) is calculated from all cells with CCDC6 knockouts and is shown as numbers on the heatmap. **f**, Two different distribution patterns of CCDC6 PS scores. **g**, The top enriched GO terms of DEG genes from PP/PP in transition. Enrichr was used to perform enrichment analysis. **h**, The percentage of cells in PP/LV/DUO cell types from CCDC6 clones. **i**, The percentage of cells with PDX1+ (a PP marker) or HNF4A+ (a LV marker) by flow cytometry sorting. The data is based on two CCDC6 knockouts (KO1, KO2) and one wild-type (WT) control. Three independent replicates are performed for each condition. The multiple comparison-adjusted p value is calculated by one-way ANOVA test. *p<0.05, **p<0.01.

Supplementary Figure Legends

Supplementary Figure S1. Benchmark different methods using simulated and real datasets. **a**, Steps to generate simulated datasets using scDesign3 from a real scRNA-seq dataset that knocks out Nelfb gene. **b-e**, The score distribution of scMAGECK-PS and mixscape using different DEG genes and different values of true efficiencies. **f-g**, Similar with Figure 1f-g, but using a published high MOI Perturb-seq dataset in the same study. **h-i**, Benchmark results of different methods on another published CRISPRi-based Perturb-seq, where mismatches are introduced into guides to attenuate perturbation effects. The Pearson correlation coefficients (PCCs) between the predicted scores of each method and the expressions of perturbed genes are reported for every perturbed gene (**h**), and between the predicted scores and predicted sgRNA activities (**i**), using the prediction methods provided in the original study²⁰.

Supplementary Figure S2. A genome-scale Perturb-seq. **a-b**, The distribution of scMAGECK-PS and mixscape predicted scores of top hits including CD247 (**a**) and LCK (**b**) in the pooled screen. **c**, The correlation between PS scores and perturbed gene expression.

Supplementary Figure S3. Predictions of PDL1 protein expression from a published ECCITE-seq dataset. The ROC curve, the correlations between scMAGECK-PS results with PDL1 protein expression, and the correlations between mixscape results with PDL1 protein expression are reported for each gene. The correlations are separated by classifications of each single cell: NP (non-perturbed), defined as mixscape score ≤ 0.5 ; and KO (knockout), defined as mixscape score > 0.5 . For a fair comparison, we used mixscape classification results to plot PS scores (mid panel).

Supplementary Figure S4. Buffered genes and sensitive genes. **a**, RPL4, a buffered gene. **b-c**, HSPA5 and GATA1, two sensitive genes. **d**, A gene (BRD4) whose expression has no correlation with PS score.

Supplementary Figure S5. The log fold changes of gene expressions upon perturbing genes within the same protein complex, including ribosomal subunits (**a**), RNA polymerase (**b**) and mediator complex (**c**) in essential gene Perturb-seq. (**d**) The log fold changes of proteosome gene expressions (columns) upon perturbing proteasome genes (rows) from the genome-scale Perturb-seq.

Supplementary Figure S6. HIV Perturb-seq. **a**, The number of genes (nFeature_RNA), UMI counts (nCount_RNA) and the fraction of mitochondrial RNAs in three different conditions. **b**, Clustering results. **c**, Enriched Gene Ontology (GO) terms of cluster 8. **d**, The distribution of BRD4-targeting gRNAs. **e**, The expression distribution of BRD4 signature genes in cluster 8 vs other clusters. Only cells express BRD4-targeting gRNAs are included. **f**, Differential expression results between BRD4 PS+ cells vs BRD4 PS- cells.

Supplementary Figure S7. HIV Perturb-seq. **a**, The expressions of CCNT1 (left) and CCNT1-targeting gRNAs (right). **b**, Differential expression results between CCNT1-targeting cells and non-targeting control cells in two different cell states. **c**, The expressions of NFKB1. **d**, The quantitative perturbation-expression relationship between GFP and CCNT1 PS score, similar with Figure 4e.

Supplementary Figure S8. Cell type assignment based on known expression markers of different cell types in pancreatic differentiation scRNA-seq.

Supplementary Figure S9. DEG analysis. **a-b**, The distribution of FOXA1 PS scores across two different clones. **c**, The expression pattern of FOXA1. **d-e**, The DEG analysis results of CCDC6 knockout clones vs. wild-type clones in different cell types. **f**, The overlap of statistically significant DEG genes in DE and LV/DUO cell types.

Supplementary Figure S10. Different CCDC6 functions. **a-b**, The two patterns of CCDC6 PS scores in LV/DUO (**a**) and DE in transition (**b**) cell types. **c-f**, Additional enriched terms using Enrichr on DEG genes of CCDC6 knockout.

Supplementary Figure S11. Flow cytometry analysis of PDX1 and HNF4A expression upon CCDC6 knockout. One representative plots of three biological replicates are shown.

Supplementary Table S1. Genome-scale Perturb-seq library design.

Supplementary Table S2. HIV Perturb-seq library design.

Supplementary Table S3. Sequencing summary of HIV Perturb-seq.

Supplementary Table S4. Genotype summary of 10-clone scRNA-seq pancreatic differentiation dataset.

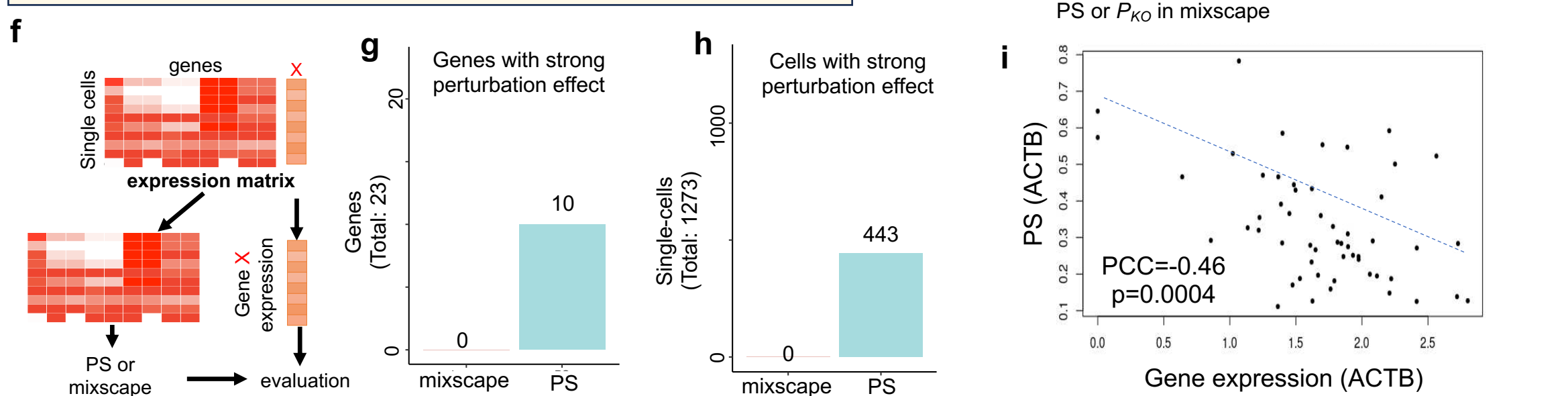
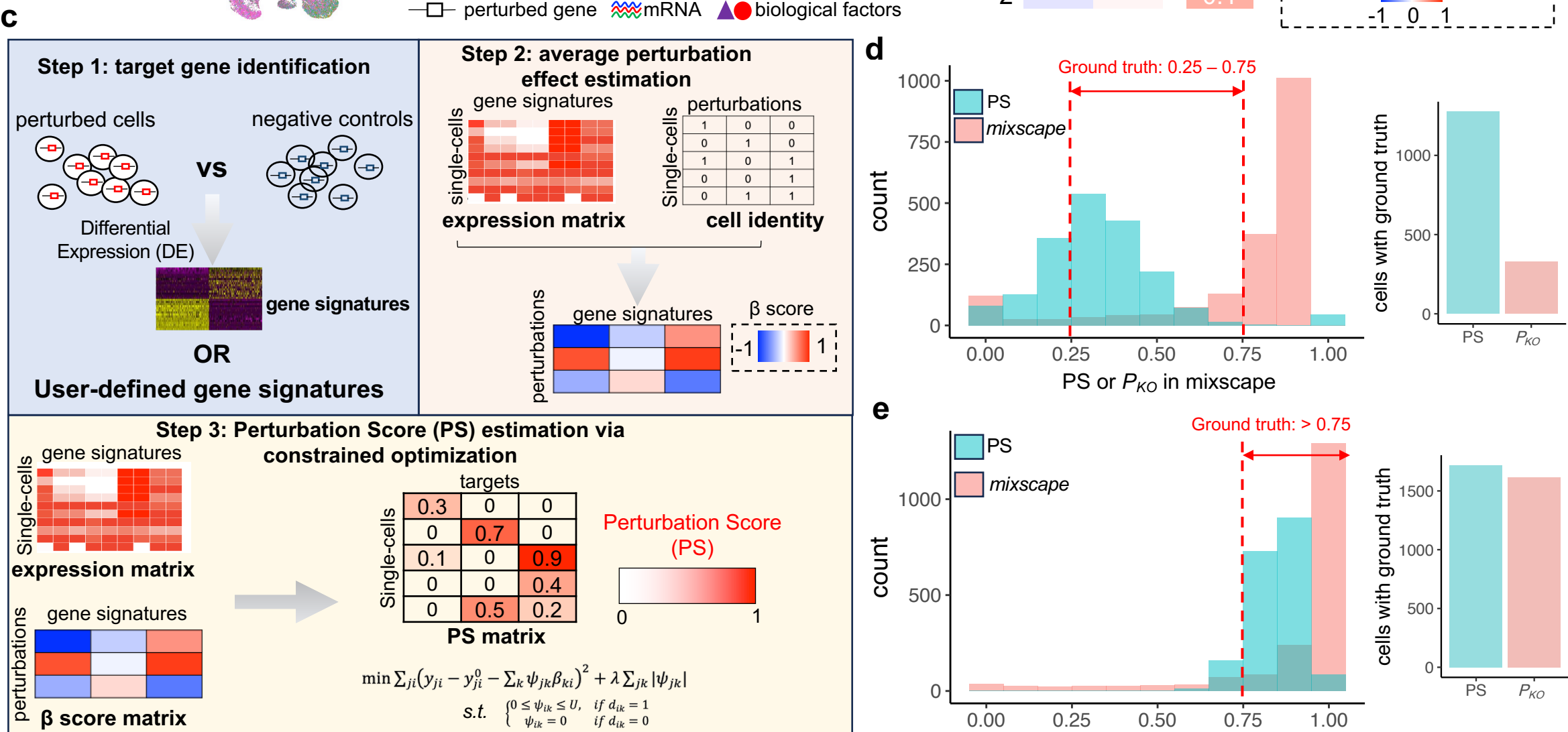
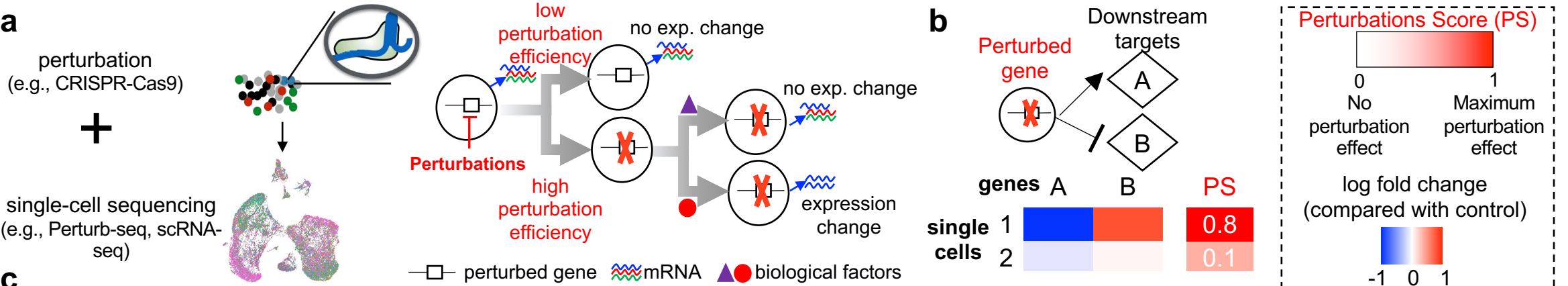


Figure 1

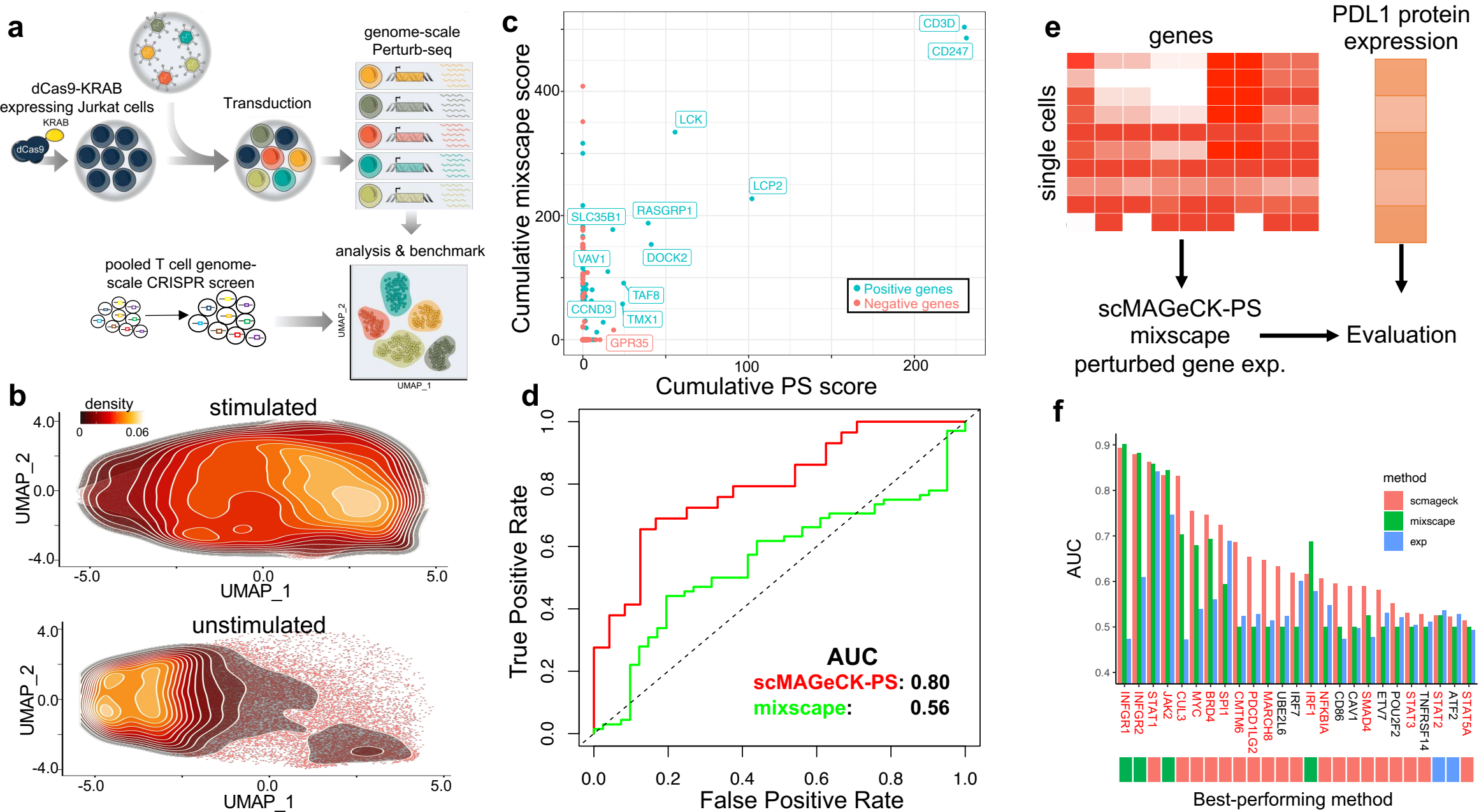


Figure 2

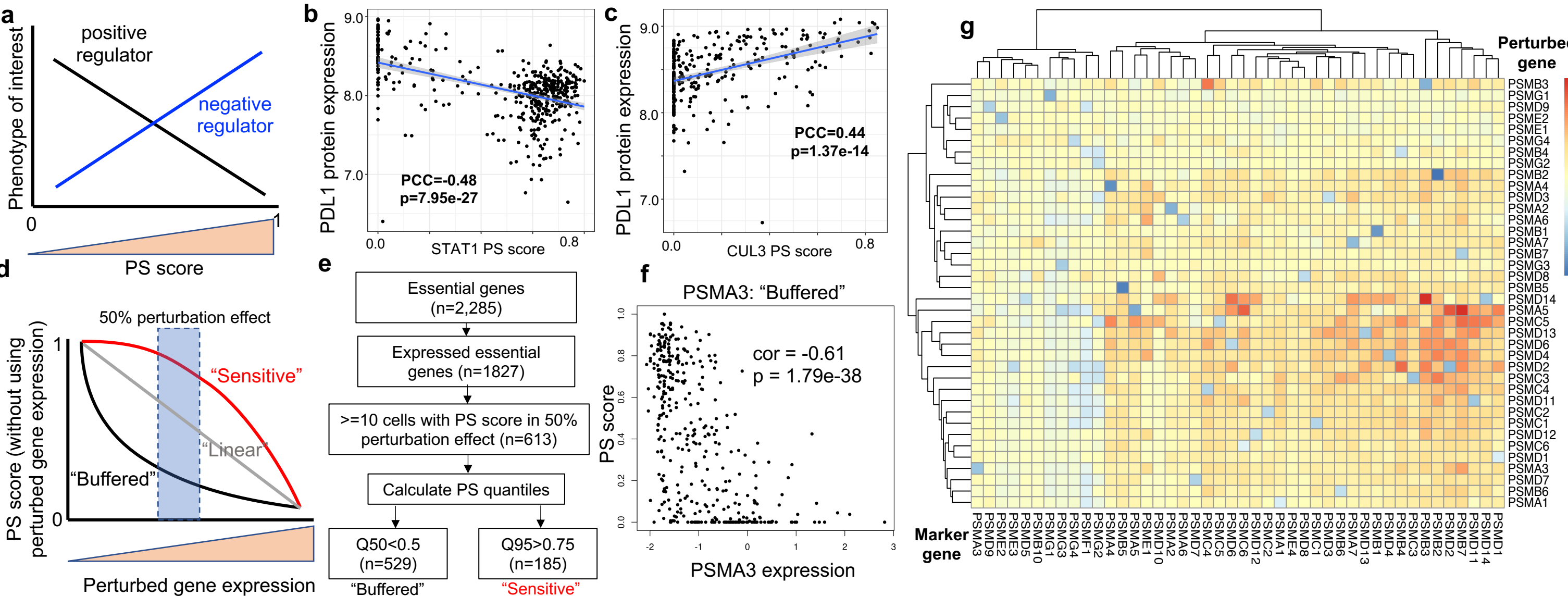


Figure 3

